

# Detecting new signals under background mismodelling\*

Sara Algeri<sup>1, †</sup><sup>1</sup>*School of Statistics, University of Minnesota, Minneapolis (MN), 55455, USA*

(Dated: August 17, 2022)

Searches for new astrophysical phenomena often involve several sources of non-random uncertainties which can lead to highly misleading results. Among these, model-uncertainty arising from background mismodelling can dramatically compromise the sensitivity of the experiment under study. Specifically, overestimating the background distribution in the signal region increases the chances of missing new physics. Conversely, underestimating the background outside the signal region leads to an artificially enhanced sensitivity and a higher likelihood of claiming false discoveries. The aim of this work is to provide a unified statistical strategy to perform modelling, estimation, inference, and signal characterization under background mismodelling. The method proposed allows to incorporate the (partial) scientific knowledge available on the background distribution and provides a data-updated version of it in a purely nonparametric fashion without requiring the specification of prior distributions. Applications in the context of dark matter searches and radio surveys show how the tools presented in this article can be used to incorporate non-stochastic uncertainty due to instrumental noise and to overcome violations of classical distributional assumptions in stacking experiments.

## I. INTRODUCTION

When searching for new physics, a discovery claim is made if the data collected by the experiment provides sufficient statistical evidence in favor of the new phenomenon. If the background and signal distributions are specified correctly, this can be done by means of statistical tests of hypothesis, upper limits and confidence intervals.

**The problem.** In practice, even if a reliable description of the signal distribution is available, providing accurate background models may be challenging, as the behavior of the sources which contribute to it is often poorly understood. Some examples include searches for nuclear recoils of weakly interacting massive particles over electron recoils backgrounds [1, 2], for gravitational-wave signals over non-Gaussian backgrounds from stellar-mass binary black holes [3], and for a standard model-like Higgs boson over prompt diphoton production [4].

Unfortunately, model uncertainty due to background mismodelling can significantly compromise the sensitivity of the experiment under study. Specifically, overestimating the background distribution in the signal region increases the chances of missing new physics. Conversely, underestimating the background outside the signal region leads to an artificially enhanced sensitivity, which can easily result in false discovery claims. Several methods have been proposed in literature to address this problem [e.g., 5–7]. However, to the best of the author’s knowledge, none of the methods available allow to (i) assess the validity of existing models for the background, (ii) fully characterize the background distribution, (iii) perform signal detection even if the signal distribution is not available, (iv) characterize the signal distribution, and (v) detect additional signals of new unexpected sources.

**Goal.** The aim of this work is to present a unified strategy which integrates modelling, estimation, and inference under background mismodelling and allows the simultaneous performance of (i)-(v). As a brief overview, given a source-free sample and the (partial) scientific knowledge available on the background distribution, a data-updated version of it is obtained in a purely nonparametric fashion without requiring the specification of prior distributions. At this stage, a graphical tool is provided in order to assess if and where significant deviations between the true and the postulated background distributions occur. The “updated” background distribution is then used to assess if the distribution of the data collected by the experiment deviates significantly from the background model. Also in this case, it is possible to assess graphically how the data distribution deviates from the expected background model. If a source-free sample is available or if control regions can be identified, the solution proposed does not require the specification of a model for the signal; however, if the signal distribution is known (up to some free parameters), the latter can be used to further improve the accuracy of the analysis and to detect the signals of unexpected new sources. The method discussed in this manuscript can be easily adjusted to cover for situations in which a source-free sample or control regions are not available, the background is unknown or incorrectly specified but a functional form of the signal distribution is known.

**The key of the solution.** The statistical methodologies involved rely on the novel *LP approach to statistical modelling* first introduced by Mukhopadhyay and Parzen in 2014 [8]. This approach allows the unification of many of the standard results of classical statistics by expressing them in terms of quantiles and comparison distributions and provides a simple and powerful framework for statistical learning and data analysis. The interested reader is directed to [9–13] and references therein, for recent advancements in mode detection, nonparametric time series, goodness-of-fit on prior distributions, and large-scale inference using an LP approach.

**Organization.** Section II is dedicated to a review of the

\* The author declares no conflict of interest.

† [salgeri@umn.edu](mailto:salgeri@umn.edu)

main constructs of LP modelling. Section III highlights the practical advantages offered by modelling background distributions using an LP approach. Section IV introduces a novel LP-based framework for statistical inference. Section V outlines the main steps of a data-scientific learning strategy for signal detection and characterization. In Section VI, the methods proposed are applied to a realistic simulation of the Fermi-LAT  $\gamma$ -ray satellite, where the source of uncertainty on the background distribution is due to ignoring the effect of the detector. Section VII is dedicated to model-denoising. Section VIII presents an application to data from the NVSS astronomical survey and discusses a simple approach to assess the validity of distributional assumptions on the polarized intensity in stacking experiments. A discussion of the main results and extensions is proposed in Section IX.

## II. LP APPROACH TO STATISTICAL MODELLING

The *LP Approach to Statistical Modelling* [8] is a novel statistical approach which provides an ideal framework to simultaneously assess the validity of the scientific knowledge available and fill the gap between the initial scientific belief and the evidence provided by the data. The main constructs of LP modelling are outlined below, whereas Section III discusses their usefulness in addressing the problem of background mis-modelling.

### A. The skew-G density model

Suppose  $x_1, \dots, x_n$  is a sample of independent and identically distributed (i.i.d.) observations from a continuous random variable  $X$ . Let  $F(x)$  and  $f(x)$  be, respectively, the cumulative distribution function (cdf) and the probability density function (pdf) of  $X$ .<sup>1</sup> Since  $F$  is the true distribution of the data, it is typically unknown. However, suppose a suitable cdf  $G(x)$  is available, and let  $g(x)$  be the respective pdf. In order to understand if  $G$  is a good candidate for  $F$ , it is convenient to express the relationship among the two in a concise manner. The *skew-G density model* [9] is a universal representation scheme defined by

$$f(x) = g(x)d(G(x); G, F) \quad (1)$$

where  $d(G(x); G, F)$  is called *comparison density* [14] and it is such that

$$d(G(x); G, F) = \frac{f(x)}{g(x)}. \quad (2)$$

Specifically, setting  $u = G(x)$  we have that  $d(u; G, F)$  corresponds to the density of the random variable  $U = G(X)$  and

<sup>1</sup> One can think of a pdf  $f(x)$  as a non-negative curve which is normalized to integrate to one, whereas its cdf corresponds to  $F(x) = \int_{-\infty}^x f(x) \partial x$ .

takes values over  $[0, 1]$ . Thus, (2) can be rewritten as

$$d(u; G, F) = \frac{f(G^{-1}(u))}{g(G^{-1}(u))} \quad \text{with } 0 \leq u \leq 1, \quad (3)$$

where  $G^{-1}(u) = \inf\{x : G(x) \geq u\}$  denotes the ‘‘postulated’’ quantile function of  $X$ . Letting  $u_i = G(x_i)$ , for  $i = 1, \dots, n$ , a sample of i.i.d. observations from  $U$  is given by  $u_1, \dots, u_n$ .

*Practical remarks.* Looking at (1), it is immediate to see that the comparison density models the departure of the true density  $f(x)$  from the postulated model  $g(x)$ . Furthermore, if  $g \equiv f$ ,  $d(u; G, F) = 1$  for all  $u \in [0, 1]$ , i.e.,  $U$  is uniformly distributed over the interval  $[0, 1]$ . Consequently, an adequate estimate of  $d(u; G, F)$ , not only leads to an estimate of the true  $f(x)$  based on (1), but it also allows to identify the regions where  $f(x)$  deviates substantially from  $g(x)$ .

### B. LP density estimate

Under the assumption that (3) is a square integrable function over the range  $[0, 1]$ , i.e.,  $d \in L_2[0, 1]$ , it is possible to represent  $d(u; G, F)$  by means of a series of normalized shifted Legendre Polynomials,<sup>2</sup> namely  $Leg_j(u)$ , with coefficients  $LP_j = \int_0^1 Leg_j(u) d(u; G, F) \partial u$ , i.e.,

$$d(u; G, F) = 1 + \sum_{j>0} LP_j Leg_j(u). \quad (4)$$

The  $LP_j$  coefficients in (4) can be estimated by

$$\widehat{LP}_j = \frac{1}{n} \sum_{i=1}^n Leg_j(u_i), \quad (5)$$

with mean  $E[\widehat{LP}_j] = LP_j$  and variance  $V(\widehat{LP}_j) = \sigma_j^2/n$ , where  $\sigma_j^2 = \int_0^1 (Leg_j(u) - LP_j)^2 d(u; G, F) \partial u$  (see [17]). Further, it can be shown [9] that, when  $f \equiv g$ ,

$$E[\widehat{LP}_j] = 0 \quad \text{and} \quad V(\widehat{LP}_j) = \frac{1}{n} \quad (6)$$

and, as  $n \rightarrow \infty$

$$\sqrt{n} \widehat{LP}_j \xrightarrow{d} N(0, 1), \quad (7)$$

where  $\xrightarrow{d}$  denotes convergence in distribution.

If (4) is approximated by the first  $M + 1$  terms,<sup>3</sup> an estimate

<sup>2</sup> Classical Legendre polynomials are defined over  $[-1, 1]$ ; here, their ‘‘shifted’’ counterpart over the range  $[0, 1]$  is considered. Finally, the shifted Legendre polynomials are normalized using the Gram-Schmidt process. The first few normalized shifted Legendre polynomials are:  $Leg_0(u) = 1$ ,  $Leg_1(u) = \sqrt{12}(u - 0.5)$ ,  $Leg_2(u) = \sqrt{5}(6u^2 - 6u + 1)$ , etc.

<sup>3</sup> Recall that the first normalized shifted Legendre polynomial is  $Leg_0(u) = 1$ .

of the comparison density is given by

$$\widehat{d}(u; G, F) = 1 + \sum_{j=1}^M \widehat{LP}_j \text{Leg}_j(u), \quad (8)$$

with standard error

$$SE \left[ \widehat{d}(u; G, F) \right] = \sqrt{\sum_{j=1}^M \frac{\widehat{\sigma}_j^2}{n} \text{Leg}_j^2(u)}, \quad (9)$$

where  $\widehat{\sigma}_j^2 = \frac{1}{n} \sum_{i=1}^n \text{Leg}_j^2(u_i) - \widehat{LP}_j^2$ .

Estimators of the form (8) are also known in literature as *sample moments approximant* [18, 19]. An important property of this class of estimators is that the respective coefficients can be specified as a linear combination of the moments of  $U$  [19]. Similarly, each  $\widehat{LP}_j$  estimate can be expressed as a linear combination of the first  $j$  sample moments of  $U$ , e.g.,

$$\widehat{LP}_2 = \frac{1}{n} \sum_{i=1}^n \text{Leg}_2(u_i) = \sqrt{5} (6\widehat{\mu}_2 - 6\widehat{\mu}_1 + 1)$$

where  $\widehat{\mu}_2 = \frac{1}{n} \sum_{i=1}^n u_i^2$ ,  $\widehat{\mu}_1 = \frac{1}{n} \sum_{i=1}^n u_i$ . Therefore, the truncation point  $M$  can be interpreted as the order of the highest moment considered to characterize the distribution of  $U$ . (The reader is directed to Section IV C for a discussion on the choice of  $M$ .)

Finally, the skew-G density model in (1) implies that

$$\widehat{f}(x) = g(x) \widehat{d}(G(x); G, F). \quad (10)$$

**Practical remarks.** Despite orthogonal polynomials being widely used tools for density estimation, when applied to  $f(x)$  directly, the analysis is limited to a mere estimation of the true pdf of the data. Conversely, in LP modelling, the shifted Legendre polynomials are of fundamental importance in revealing the scientific insights enclosed in  $d(u; G, F)$ . In this respect,  $\widehat{d}(u; G, F)$  plays the role of an ‘‘oracle’’ distribution which provides a deeper understanding of the sensitivity of the analysis and enriches the scientist’s knowledge on the nature of both the signal and the background distribution. This sets the ground for a novel *data-scientific learning* framework in which the data and the scientist iteratively learn from each other, and ‘‘convergence of the solution’’ is achieved when a mutual agreement between data-driven and scientific knowledge is reached (see Section V).

### III. DATA-DRIVEN CORRECTIONS FOR MISSPECIFIED BACKGROUND MODELS

Let  $\mathbf{x} = (x_1, \dots, x_n)$  be a data sample on which we would like to assess whether the signal of interest is present or not. Suppose that, in addition to  $\mathbf{x}$ , a source-free dataset  $\tilde{\mathbf{x}} = (\tilde{x}_1, \dots, \tilde{x}_N)$  is given. The latter may be a sample of observations from control regions or the result of Monte Carlo simulations, assuming that no signal is present. Hereafter, re-

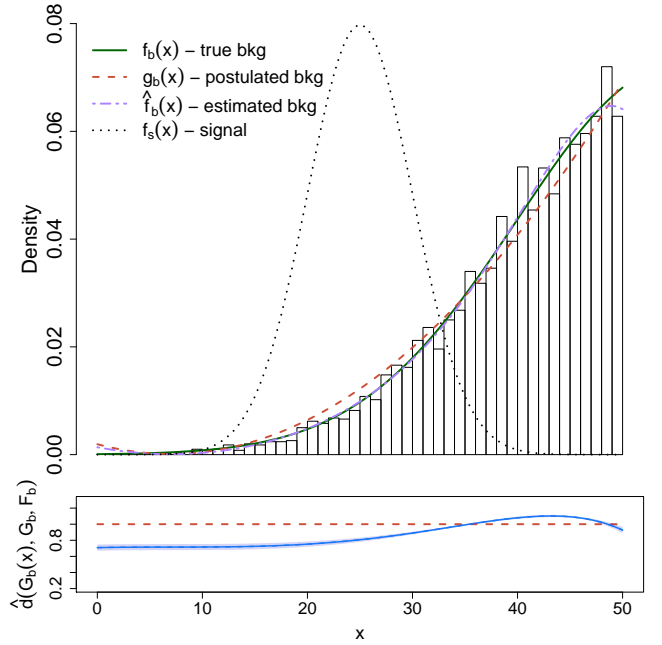


FIG. 1: Upper panel: histogram of a source-free sample simulated from the tail of a Gaussian with mean 55 and width 15 (green solid line). The candidate background distribution is given by the best fit of a second-degree polynomial (red dashed line), and it is updated using the source-free data by means of (14) (purple chained line). Bottom panel: comparison density estimate (blue solid line) plotted on the  $x$ -scale and respective standard errors (light blue area) computed as in (9).

fer to  $\mathbf{x}$  as the *physics sample* and to  $\tilde{\mathbf{x}}$  as the *source-free sample*. Notice that, if no source is present, both  $\tilde{\mathbf{x}}$  and  $\mathbf{x}$  are distributed according to  $f_b(x)$ . Therefore,  $\tilde{\mathbf{x}}$  can be used to ‘‘learn’’ the unknown pdf of the background, namely  $f_b(x)$ .

Despite the true background model being unknown, suppose that a candidate pdf, namely  $g_b(x)$ , is available. The candidate model  $g_b(x)$  can be specified from previous experiments or theoretical results or can be obtained by fitting specific functions (e.g., polynomial, exponential, etc.) to  $\tilde{\mathbf{x}}$ . If  $g_b(x)$  does not provide an accurate description of  $f_b(x)$ , the sensitivity of the experiment can be strongly affected.

Consider, for instance, a source-free sample of  $N = 5000$  observations whose true (unknown) distribution corresponds to the tail of a Gaussian with mean 55 and width 15 over the range  $[0, 50]$ , i.e.,

$$f_b(x) = \frac{e^{-\frac{1}{2} \left( \frac{x-55}{15} \right)^2}}{k_{fb}} \quad (11)$$

with  $k_{fb} = \int_0^{50} e^{-\frac{1}{2} \left( \frac{x-55}{15} \right)^2} \partial x$ . Suppose that a candidate model for the background is obtained by fitting a second-degree polynomial on the source-free sample and adequately normal-

izing it in order to obtain a proper pdf, i.e.,

$$g_b(x) = \frac{9.52 - 2.22x + 0.15x^2}{k_{gb}} \quad (12)$$

with  $k_{gb} = \int_0^{50} [9.52 - 2.22x + 0.15x^2] \partial x$ . For illustrative purposes, assume that the distribution of the signal is a Gaussian centered at 25, with width 4.5 and pdf

$$f_s(x) = \frac{e^{-\frac{1}{2}\left(\frac{x-25}{4.5}\right)^2}}{k_{fs}} \quad (13)$$

with  $k_{fs} = \int_0^{50} e^{-\frac{1}{2}\left(\frac{x-25}{4.5}\right)^2} \partial x$ . The histogram of the source-free sample along with (11)-(13) is shown in Fig. 1. At the higher end of the spectrum, the postulated background (red dashed line) underestimates the true background distribution (green solid line). As a result, using (12) as background model increases the chance of false discoveries in this region. Conversely, at the lower end of the spectrum,  $g_b(x)$  underestimates  $f_b(x)$ , reducing the sensitivity of the analysis.

It is important to point out that, the discrepancy of  $f_b(x)$  from  $g_b(x)$  is typically due to the fact that the specific functional form imposed (in our example, a second-degree polynomial) is not adequate for the data. Thus, changing the values of the fitted parameters (or assigning priors to them) is unlikely to solve the problem. However, it is possible to “repair”  $g_b(x)$  and obtain a suitable estimate of  $f_b(x)$  by means of (10). Specifically,  $f_b(x)$  can be estimated via

$$\hat{f}_b(x) = g_b(x) \hat{d}(G_b(x); G_b, F_b) \quad (14)$$

where  $\hat{d}(G_b(x); G_b, F_b)$  is the comparison density estimated via (8) on the sample  $G_b(\tilde{x}_1), \dots, G_b(\tilde{x}_N)$ , whereas  $F_b$  and  $G_b$  are the true and the postulated background distributions, with pdfs as in (11) and (12), respectively.

In our example, choosing  $M = 2$  (see Section IV C), we obtain

$$\hat{d}(G_b(x); G_b, F_b) = 1 + 0.063 \text{Leg}_1[G_b(x)] - 0.082 \text{Leg}_2[G_b(x)], \quad (15)$$

where  $\text{Leg}_1[G_b(x)]$  and  $\text{Leg}_2[G_b(x)]$  are the first and second normalized shifted Legendre polynomials evaluated at  $G_b(x)$ . Notice that, by combining (14) and (15), we can easily write the background model using of a series of shifted Legendre polynomials. This may be especially useful when dealing with complicated likelihoods and for which a functional form is difficult to specify.

The upper panel of Fig. 1 shows that the “calibrated” background model in (14) as a purple chained line and matches almost exactly the true background density in (11) (green solid line). The plot of  $\hat{d}(G_b(x); G_b, F_b)$  in the bottom panel of Fig. 1 provides important insights on the deficiencies of (12) as a candidate background model. Specifically, the magnitude and the direction of the departure of  $\hat{d}(G_b(x); G_b, F_b)$  from one corresponds to the estimated departure of  $f_b(x)$  from  $g_b(x)$  for each value of  $x$ . Therefore, if  $\hat{d}(G_b(x); G_b, F_b)$  is below

one in the region where we expect the signal to occur, using  $\hat{f}_b(x)$  in place of  $g_b(x)$  increases the sensitivity of the analysis. Conversely, if  $\hat{d}(G_b(x); G_b, F_b)$  is above one outside the signal region, the use of  $\hat{f}_b(x)$  instead of  $g_b(x)$  prevents from false discoveries.

Notice that in this article we only consider continuous data. In this respect, the goal is to learn the model of the background considered as a continuum and no binning is applied. Therefore, the histograms presented here are only a graphical tool used to display the data distribution and are not intended to represent an actually binning of the data.

#### IV. LP-BASED INFERENCE

When discussing the skew-G density model in (1), we have witnessed that  $f \equiv g$  if  $d(u; G, F) = 1$  for all  $u \in [0, 1]$ . Additionally, the graph of  $\hat{d}(u; G, F)$  provides an exploratory tool to understand the nature of the deviation of  $f(x)$  from  $g(x)$ . This section introduces a novel inferential framework to test the significance of the departure of  $f(x)$  from  $g(x)$ . Specifically, we aim to test the hypotheses

$$\begin{aligned} H_0 : d(u; G, F) = 1 \text{ for all } u \in [0, 1] \\ \text{vs} \\ H_1 : d(u; G, F) \neq 1 \text{ for some } u \in [0, 1]. \end{aligned} \quad (16)$$

First, an overall test, namely the *deviance test*, is presented. The deviance test assesses if  $f(x)$  deviates significantly from  $g(x)$  anywhere over the range of  $x$  considered. Second, adequate confidence bands are constructed in order to assess where significant departures occur.

##### A. The deviance test

The quantity  $\sum_{j=1}^M \widehat{LP}_j^2$  is known as *deviance* [12] and quantifies the departure of  $\hat{d}(u; G, F)$  from one. If the deviance is equal to zero, we may expect that  $g$  is approximately equivalent to  $f$ ; hence, we test

$$H_0 : \sum_{j=1}^M LP_j^2 = 0 \quad \text{vs} \quad H_1 : \sum_{j=1}^M LP_j^2 > 0 \quad (17)$$

by means of the test statistic

$$D_M = n \sum_{j=1}^M \widehat{LP}_j^2. \quad (18)$$

From (7) it follows that, under  $H_0$ ,  $D_M$  is asymptotically  $\chi_M^2$ -distributed; hence, an asymptotic p-value for (17) is given by

$$P(D_M > d_M) \xrightarrow{n \rightarrow \infty} P(\chi_M^2 > d_M), \quad (19)$$

where  $d_M$  is the value of  $D_M$  observed on the data.

*Practical remarks.* Notice that  $H_1$  in (17) implies  $H_1$  in (16). Similarly,  $H_0$  in (16) implies  $H_0$  in (17); however, the opposite is not true in general since there may be some non-zero  $LP_j$  coefficients for  $j > M$ . Therefore, choosing  $M$  small may lead to conservative, but yet valid, inference.

## B. Confidence bands

The estimator in (8) only accounts for the first  $M + 1$  terms of the polynomial series in (4). Therefore,  $\hat{d}(u; G, F)$  is a biased estimator of  $d(u; G, F)$ . Specifically, its bias, namely  $B[\hat{d}(u; G, F)]$ , is given by

$$B[\hat{d}(u; G, F)] = \sum_{j>M} LP_j Leg_j(u) \quad (20)$$

for  $u \in [0, 1]$ . As a result, when (20) is large, confidence bands based on  $\hat{d}(u; G, F)$  are shifted away from the true density  $d(u; G, F)$ . Despite the bias cannot be easily quantified in the general setting, it follows from (6) that, when  $H_0$  in (16) is true,  $B[\hat{d}(u; G, F)] = 0$ . Thus, we can exploit this property to construct reliable confidence bands under the null. Specifically, the goal is to identify  $c_\alpha$ , such that

$$\begin{aligned} 1 - \alpha &= P(-c_\alpha \leq \hat{d}(u; G, F) - 1 \leq c_\alpha, \text{ for all } u \in [0, 1] | H_0) \\ &= P(\max_u |\hat{d}(u; G, F) - 1| \leq c_\alpha | H_0) \end{aligned} \quad (21)$$

where  $\alpha$  is the desired significance level.<sup>4</sup>

If the bias determines where the confidence bands are centered, the distribution and the variance of  $\hat{d}(u; G, F)$  determine their width. Under  $H_0$ , the standard error of in (9) reduces to

$$SE[\hat{d}(u; G, F)] = \sqrt{\sum_{j=1}^M \frac{1}{n} Leg_j^2(u)}. \quad (22)$$

Additionally, (7) implies that  $\hat{d}(u; G, F)$  is asymptotically normally distributed, hence

$$\frac{\hat{d}(u; G, F) - 1}{\sqrt{\sum_{j=1}^M \frac{1}{n} Leg_j^2(u)}} \xrightarrow{d} N(0, 1). \quad (23)$$

as  $n \rightarrow \infty$ , for all  $u \in [0, 1]$ , under  $H_0$ .

We can then construct confidence bands under  $H_0$  which satisfy (21) by means of tube formulae (see [17, Ch.5] and

[20]), i.e.,

$$\left[ 1 - c_\alpha \sqrt{\sum_{j=1}^M \frac{1}{n} Leg_j^2(u)}, 1 + c_\alpha \sqrt{\sum_{j=1}^M \frac{1}{n} Leg_j^2(u)} \right], \quad (24)$$

where  $c_\alpha$  is the solutions of

$$2(1 - \Phi(c_\alpha)) + \frac{k_0}{\pi} e^{-0.5c_\alpha^2} = \alpha, \quad (25)$$

with  $k_0 = \sqrt{\sum_{j=1}^M [\frac{\partial}{\partial u} Leg_j(u)]^2}$ . If  $\hat{d}(u; G, F)$  is within the bands in (24) over the entire range  $[0, 1]$ , we conclude that there is no evidence that  $f$  deviates significantly from  $g$  anywhere over the range considered. Conversely, we expect significant departures to occur in regions where  $\hat{d}(u; G, F)$  lies outside the confidence bands.

*Practical remarks.* Equations (9) and (20), together, imply that, as  $M$  increases, the bias of  $\hat{d}(u; G, F)$  decreases while its variance inflates since more and more terms contribute to it. However, when  $H_0$  in (16) is true,  $B[\hat{d}(u; G, F)] = 0$ , regardless of the choice of  $M$ . This implies that the confidence bands in (24) are only affected by the variance and asymptotic distribution of  $\hat{d}(u; G, F)$  under  $H_0$ .

## C. Choice of $M$

The number of  $\widehat{LP}_j$  estimates considered determines the smoothness of  $\hat{d}(u; G, F)$ , with smaller values of  $M$  leading to smoother estimates. The deviance test can be used to select the value  $M$  which maximizes the sensitivity of the analysis according to the following scheme:

- i. Choose a sufficiently large value  $M_{\max}$ .
- ii. Obtain the estimates  $\widehat{LP}_1, \dots, \widehat{LP}_{M_{\max}}$  as in (5).
- iii. For  $m = 1, \dots, M_{\max}$ :

calculate the deviance test p-value as in (19), i.e.,

$$p(m) = P(\chi_m^2 > d_m) \quad (26)$$

with  $d_m = n \sum_{j=1}^m \widehat{LP}_j^2$ .

- iv. Choose  $M$  such that

$$M = \underset{m}{\operatorname{argmin}} \{p(m)\}. \quad (27)$$

### 1. Adjusting for post-selection

As any data-driven selection process, the scheme presented above affects the distribution of (8) and can yield to overly optimistic inference [21, 22]. Despite this aspect being often

<sup>4</sup> In astrophysics, the statistical significance  $\alpha$  is often expressed in terms of number of  $\sigma$ -deviations from the mean of a standard normal, namely  $\sigma$ . For instance, a  $2\sigma$  significance corresponds to  $\alpha = 1 - \Phi(2) = 0.0227$ , where  $\Phi(\cdot)$  denotes the cdf of a standard normal.



ignored in practical applications, correct coverage can only be guaranteed if adequate corrections are implemented. In our setting, the number of models under comparison is typically small ( $M_{\max} \leq 20$ ); therefore, post-selection inference can be easily adjusted by means of Bonferroni's correction [23]. Specifically, the adjusted deviance p-value is given by

$$M_{\max} \cdot P(\chi_M^2 > d_M), \quad (28)$$

where  $M$  is the value selected via (27), whereas confidence bands can be adjusted by substituting  $c_\alpha$  in (24), with  $c_{\alpha, M_{\max}}$  satisfying

$$2(1 - \Phi(c_{\alpha, M_{\max}})) + \frac{k_0}{\pi} e^{-0.5c_{\alpha, M_{\max}}^2} = \frac{\alpha}{M_{\max}}. \quad (29)$$

Notice that, since Bonferroni's correction leads to an upper bound for the overall significance, the resulting coverage will be higher than the nominal one. Alternatively, approximate post-selection confidence bands and inference can be constructed using Monte Carlo and/or resampling methods and repeating the selection process at each replicate.

*Practical remarks.* As noted in Section II, the estimate (8) involves the first  $M$  sample moments of  $U$ ; therefore,  $M_{\max}$  can be interpreted as the order of the highest moment which we expect to contribute in discriminating the distribution of  $U$  from uniformity. As a rule of thumb,  $M_{\max}$  is typically chosen  $\leq 20$ . Finally, Steps i-iv aim to select the approximant based on the first most significant  $M$  moments, while excluding powers of higher order. A further note on model-denoising is given in Section VII.

## V. A DATA-SCIENTIFIC APPROACH TO SIGNAL SEARCHES

The tools presented in Sections II and IV provide a natural framework to simultaneously

- assess the validity of the postulated background model and, if necessary, update it using the data (Section III);
- perform signal detection on the physics sample;
- characterize the signal when a model for it is not available.

Furthermore, if the model for the signal is known (up to some free parameters), it is possible to

- further refine the background or signal distribution;
- detect hidden signals from new unexpected sources.

Tasks (a)-(e) can be tackled in two main phases. In the first phase, the postulated background model is ‘‘calibrated’’ on a source-free sample in order to improve the sensitivity of the analysis and reduce the risk of false discoveries. The second phase focuses on searching for the signal of interest and involves both a nonparametric signal detection stage and a semi-parametric stage for signal characterization. Both phases and

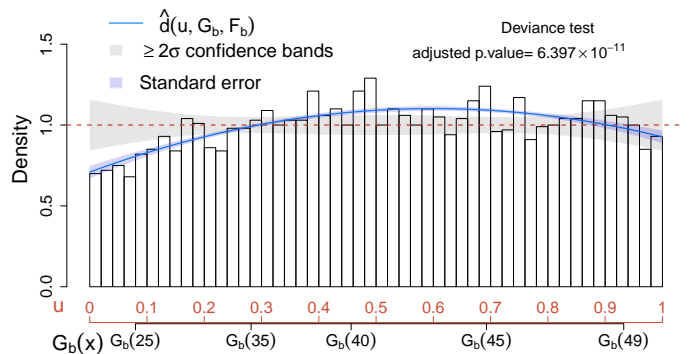


FIG. 2: Deviance test and CD plot for the source-free sample. The comparison density is estimated via (15) (solid blue line), and its standard error (light blue area) is computed according to (9). Finally, confidence bands have been constructed around one (grey areas) via (24) with  $c_\alpha$  replaced by  $c_{\alpha, M_{\max}}$  in (44). The notation  $\geq 2\sigma$  is used to highlight that Bonferroni's correction has been applied to adjust for post-selection inference, leading to an increase of the nominal coverage.

respective steps are described in details below and summarized in Algorithm 1.

### A. Background calibration

As discussed in Section III, deviations of  $\hat{d}(G_b(x); G_b, F_b)$  from one suggest that a further refinement of the candidate background model  $g_b$  is needed. However, as  $M$  increases, the deviations of  $\hat{d}(G_b(x); G_b, F_b)$  from one may become more and more prominent while the variance inflates. Thus, it is important to assess if such deviations are indeed significant. In order address this task, the analysis of Section III can be further refined in light of the inferential tools introduced in Section IV.

For the toy example discussed in Section III, we have seen that  $g_b$  overestimates  $f_b$  in the signal region and underestimates it at the higher end of the range considered (Fig. 1). We can now assess if any of these deviations are significant by implementing the deviance test in (18)-(19), whereas, to identify where the most significant departures occur, we construct confidence bands under the null model as in (24), i.e., assuming that no ‘‘update’’ of  $g_b$  is necessary.

The results are collected in the *comparison density plot* or *CD plot* presented in Fig. 2. First, a value  $M = 2$  has been selected as in (27), and the respective deviance test (adequately adjusted via Bonferroni) indicates that the deviation of  $f_b$  from  $g_b$  is significant at a  $6.430\sigma$  significance level (adjusted p-value of  $6.399 \cdot 10^{-11}$ ). Additionally, the estimated comparison density in (15) lies outside the  $2\sigma$  confidence bands in the region  $[0, 50]$  where the signal specified in (13) is expected to occur; hence, using (14) instead of (12) is recommended in order to improve the sensibility of the analysis in the signal region.

---

**Algorithm 1:** a data-scientific signal search
 

---

**INPUTS:** source-free sample  $\tilde{x}$ ;  
 postulated background distribution  $g_b(x)$ ;  
 physics sample  $\mathbf{x}$ .  
*If available:* signal distribution,  $f_s(x, \theta_s)$ .

**PHASE A: background calibration**

*Step 1:* Estimate  $\hat{d}(u; G_b, F_b)$  on  $\tilde{u} = G_b(\tilde{x})$  and test (16) via deviance test and CD plot.

*Step 2:* **if**  $F_b \neq G_b$ , set  $\hat{f}_b(x) = g_b(x)\hat{d}(u; G_b, F_b)$ ;  
**else** set  $\hat{f}_b(x) = g_b(x)$ .

**PHASE B: signal search**

**Stage 1: nonparametric signal detection**

*Step 3:* set  $g(x) = \hat{f}_b(x)$ .

*Step 4:* estimate  $\hat{d}(u; G, F)$  on  $\mathbf{u} = G(\mathbf{x})$  and test (16) via deviance test and CD plot.

*Step 5:* **if**  $G \neq F$ , claim evidence in favor of the signal and go to Step 6;  
**else** set  $\hat{f}(x) = g(x)$ , claim that no signal is present and stop.

**Stage 2: semiparametric signal characterization**

*Step 6:* **if**  $f_s(x, \theta_s)$  given, fit  $g_{bs}(x)$  in (33);  
**else** use the CD plot of  $\hat{d}(u; G, F)$  and the theory available to specify/fit a suitable model for  $f_s(x, \theta_s)$  and fit  $g_{bs}(x)$  in (33).

*Step 7:* estimate  $\hat{d}(u; G_{bs}, F)$  on  $\mathbf{u} = G_{bs}(\mathbf{x})$  and test (16) via deviance test and CD plot.

*Step 8:* **if**  $G_{bs} \neq F$ , claim evidence of unexpected signal and use the CD plot of  $\hat{d}(u; G_{bs}, F)$  and the theory available to further investigate the nature the deviation from  $G_{bs}$ ;  
**else** go to Step 9.

*Step 9:* compute  $\hat{d}(u; G, F)$  as in (34) and use it to refine  $\hat{f}_b(x)$  or  $f_s(x, \theta_s)$  as in (35). Go back to Step 3.

---

*Important remarks on the CD plot.* When comparing different models for the background or when assessing if the data distribution deviates from the model expected when no signal is present (see Section VB 1), it is common practice to visualize the results of the analysis by superimposing the models under comparison to the histogram of the data observed on the original scale (e.g., upper panel of Fig. 1). This corresponds to a data visualization in the density domain. Conversely, the CD plot (e.g., Fig. 2) provides a

representation of the data in the comparison density domain, which offers the advantage of connecting the true density of the data with the quantiles of the postulated model (see (3)). Consequently, the most substantial departures of the data distribution from the expected model are magnified, and those due to random fluctuations are smoothed out (see, also, Section VB 2). Furthermore, the deviance tests and the CD plot together provide a powerful goodness-of-fit tool and exploratory which, conversely from classical methods such as Anderson-Darling [15] and Shapiro-Wilk [16], not only allow to test if the distributions under comparison differ, but they also allow to assess how and where they differ. As a result, the CD plot can be used to characterize the unknown signal distribution (see Section VB 2) and to identify exclusion regions (e.g., Case I in Section VB 1).

*Reliability of the calibrated background model.* The size  $N$  of the source-free sample plays a fundamental role in the validity of  $\hat{f}_b(x)$  as a reliable background model. Specifically, the randomness involved in (14) only depends on the  $\widehat{LP}_j$  estimates. If  $N$  is sufficiently large, by the strong law of large numbers,

$$P\left(\lim_{N \rightarrow \infty} \widehat{LP}_j = LP_j\right) = 1.$$

Therefore, despite the variance of  $\hat{f}_b(x)$  becoming negligible as  $N \rightarrow \infty$ , one has to account for the fact that  $\hat{f}_b(x)$  leads to a biased estimate of  $f_b(x)$  when  $f_b \neq g_b$  (see Section IV B). For sufficiently smooth densities, a visual inspection is often sufficient to assess if  $\hat{d}(u; G_b, F_b)$  (and, consequently,  $\hat{f}_b(x)$ ) provides a satisfactory fit for the data, whereas, for more complex distributions the effect of the bias can be mitigated considering larger values of  $M$  and model-denoising (see Section VII A).

## B. Signal search

### 1. Nonparametric signal detection

The background calibration phase allows the specification of a well tailored model for the background, namely  $\hat{f}_b(x)$ , which simultaneously integrates the initial guess,  $g_b$ , and the information carried by the source-free data sample. Hereafter, we disregard the source-free data sample and focus on analyzing the physics sample.

Under the assumption that the source-free sample has no significant source contamination, we expect that, if the signal is absent, both the source-free and the physics sample follow the same distribution. Therefore, the calibrated background model,  $\hat{f}_b(x)$ , plays the role of the postulated distribution for the physics sample, i.e., the model that we expect the data to follow when no signal is present; hence, we set  $g(x) = \hat{f}_b(x)$ .

Let  $f(x)$  be the (unknown) true pdf of the physics sample which may or may not carry evidence in favor of the source of interest. When no model for the signal is specified, it is reasonable to consider any significant deviation of  $f$  from  $g$  as an indication that a signal of unknown nature may be present.

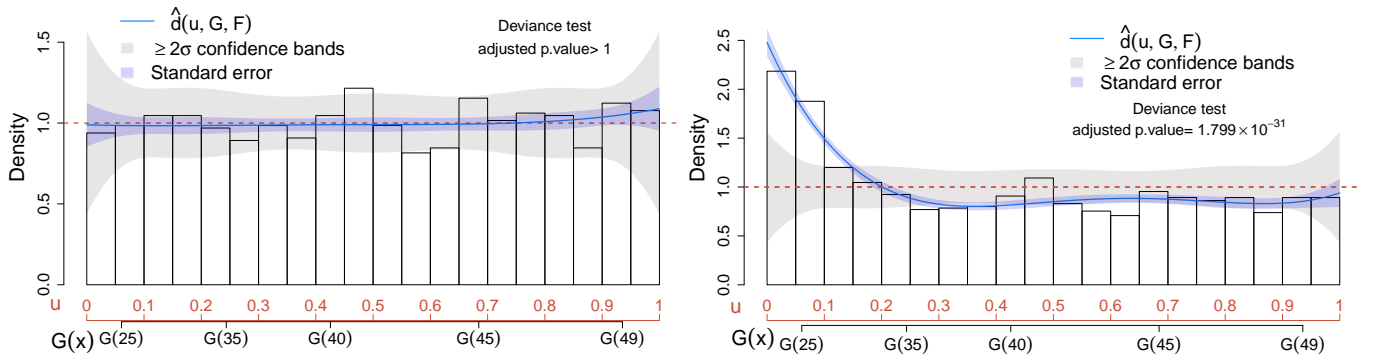


FIG. 3: Deviance test and CD plots for Case I where no signal is present (left panel) and Case II where the signal is present (right panel). In both cases, the postulated distribution  $G$  corresponds to the cdf of the calibrated background model in (30). For the sake of comparison,  $d(u; G, F)$  has been estimated via (8) with  $M = 4$  for both samples.

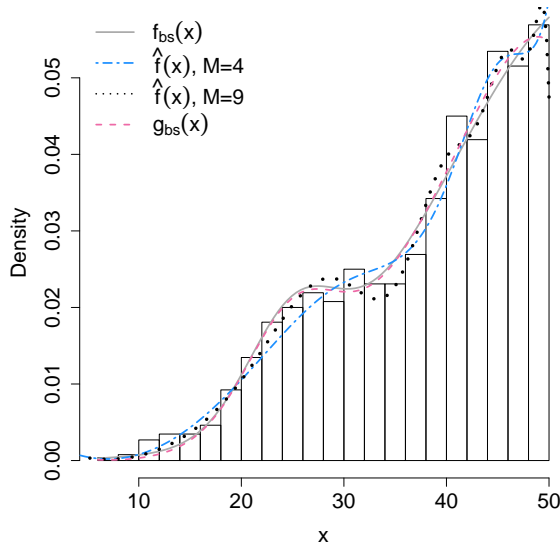


FIG. 4: Histogram of a physics sample of  $n = 1300$  observations from both background and signal and with pdf as in (31) (grey solid line). The true density has been estimated semiparametrically, as in (33) (pink dashed line), whereas the nonparametric estimates of  $f(x)$  have been computed as in (10), by plugging-in the  $\hat{d}(G(x); G, F)$  estimates obtained with  $M = 4$  (blue chained line) and  $M = 9$  (black dotted line).

In this setting, similarly to the background calibration phase, we can construct deviance tests and CD plots to assess if and where significant departures of  $f$  from  $g$  occur. Two possible scenarios are considered – a physics sample which collects only background data (Case I) and a physics sample of observations from both background and signal (Case II).

**Case I: background-only.** Let  $x$  be a physics sample of  $n = 1300$  observations whose true (unknown) pdf  $f(x)$  is

equivalent to  $f_b(x)$  in (11). We set

$$g(x) = \hat{f}_b(x) = g_b(x)\hat{d}(G_b(x); G_b, F_b) \quad (30)$$

where  $g_b(x)$  and  $\hat{d}(G_b(x); G_b, F_b)$  are defined as in (12) and (15), respectively. The resulting CD plot and deviance test are reported in the left panel of Fig. 3.

When applying the scheme in Section IV C with  $M_{\max} = 20$ , none of the values of  $M$  considered lead to significant results; therefore, for the sake of comparison with Case II below, we choose  $M = 4$ . Not surprisingly, the estimated comparison density approaches one over the entire range and lies entirely within the confidence bands. This suggests that the true distribution of the data does not differ significantly from the model which accounts only for the background. Similarly, the deviance test leads to very low significance (adjusted p-value  $> 1$ ); hence, we conclude that our physics sample does not provide evidence in favor of the new source.

**Case II: background + signal.** Let  $x$  be a physics sample of  $n = 1300$  observations whose true (unknown) pdf  $f(x)$  is equal to  $f_{bs}(x)$  in (31)

$$f_{bs}(x) = (1 - \eta)f_b(x) + \eta f_s(x) \quad (31)$$

with  $f_b(x)$  and  $f_s(x)$  defined as in (11) and (13) respectively, and  $\eta = 0.15$ . The histogram of the data and the graph of  $f_{bs}(x)$  are plotted in Fig. 4. As in Case I, we set  $g(x)$  as in (30).

The CD plot and deviance test in the right panel of Fig. 3 show a significant departure of the data distribution from the background-only model in (30). The maximum significance of the deviance is achieved at  $M = 4$ , leading to a rejection of the null hypothesis at a  $11.61\sigma$  significance level (adjusted p-value =  $1.799 \cdot 10^{-31}$ ). The CD plot shows a prominent peak at the lower end of the spectrum; hence, we conclude that there is evidence in favor of the signal, and we proceed to characterize its distribution as described in Section V B 2.



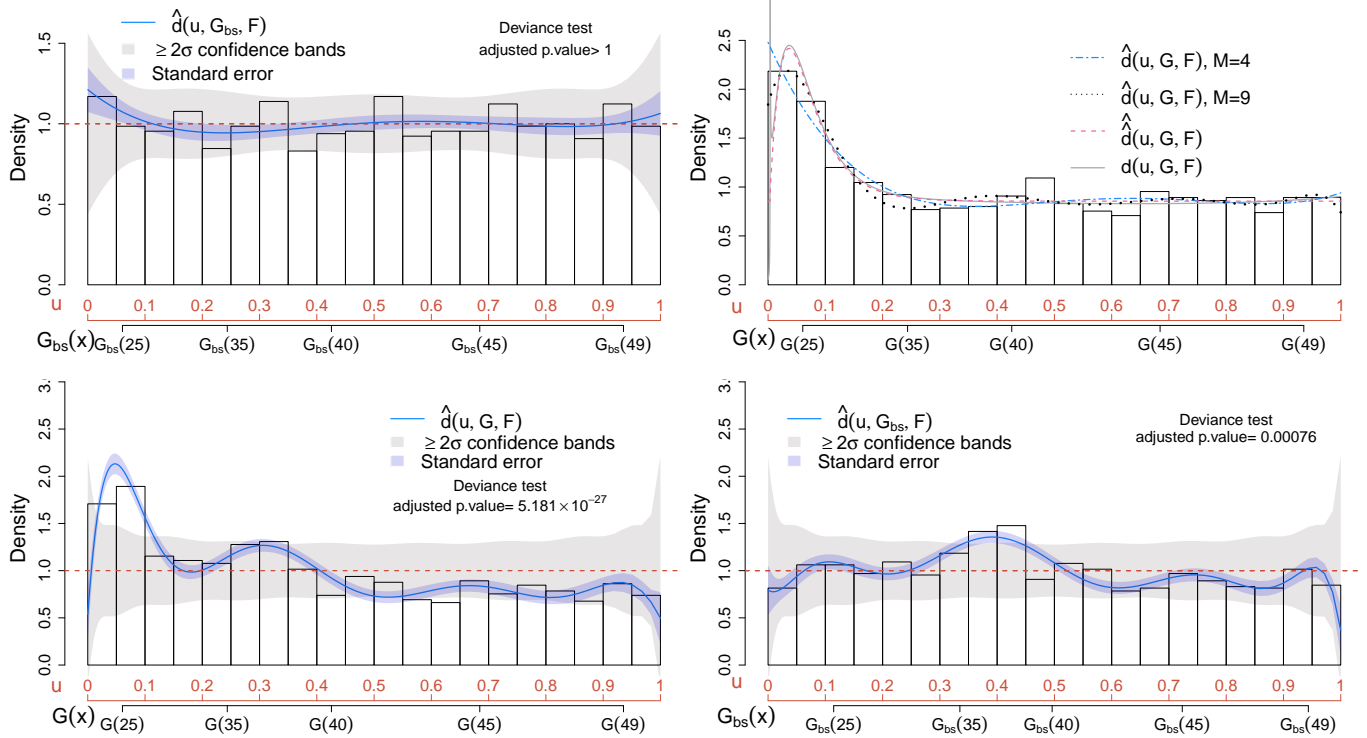


FIG. 5: Upper panels: deviance test and CD plots for Case IIa where the signal is present (right panel), and the postulated distribution  $G_{bs}$  corresponds to the cdf of the estimated background+signal model in (33) with  $\hat{\eta} = 0.146$ . The comparison density estimate has been obtained considering  $M = 3$ . Bottom panels: Deviance test and CD plots for Case III where, in addition to the signal of interest, an additional resonance is present. The data are first analyzed considering the background-only pdf in (12) as the postulated model (left panel). The analysis is then repeated by assuming the fitted background + signal model in (33) as the postulated distribution (right panel). Both estimates of the comparison density in the left and right panels have been computed as in (8) with  $M = 9$ .

## 2. Semiparametric signal characterization

The signal detection strategy proposed in Section VB1 does not require the specification of a distribution for the signal. However, if a model for the signal is known (up to some free parameters), the analysis can be further refined by providing a parametric estimate of the comparison density and assessing if additional signals from new unexpected sources are present.

**Case IIa: background + (known) signal.** Assume that a model for the signal,  $f_s(x, \theta_s)$ , is given, with  $\theta_s$  being a vector of unknown parameters. Since the CD plot in the right panel of Fig. 3 provides evidence in favor of the signal, we expect the data to be distributed according to the pdf

$$\hat{f}_{bs}(x) = (1 - \hat{\eta})\hat{f}_b(x) + \hat{\eta}f_s(x, \hat{\theta}_s), \quad 0 \leq \hat{\eta} \leq 1, \quad (32)$$

where  $\hat{f}_b(x)$  is the calibrated background distribution in (30) and  $\hat{\eta}$  and  $\hat{\theta}_s$  can be estimated via Maximum Likelihood (ML). Letting  $\hat{\eta}$  and  $\hat{\theta}_s$  be the ML estimates of  $\eta$  and  $\theta_s$  respectively, we specify

$$g_{bs}(x) = (1 - \hat{\eta})\hat{f}_b(x) + \hat{\eta}f_s(x, \hat{\theta}_s) \quad (33)$$

as postulated model. For simplicity, let  $f_s$  to be fully specified as in (13); we construct the deviance test and the CD plot to assess if (33) deviates significantly from the true distribution of the data. The scheme in Section IV C has been implemented with  $M_{\max} = 20$ , and none of the values of  $M$  considered led to significant results. The CD plot and deviance test for  $M = 4$  are reported in the upper left panel of Fig. 5. Both the large p-value of the deviance test (adjusted p-value > 1) and the CD plot suggest that no significant deviations occur; thus, (33) is a reliable model for the physics sample.

Furthermore, we can use (33) to further refine our  $\hat{f}_b(x)$  or  $f_s(x, \hat{\theta}_s)$  distributions. Specifically, we first construct a semi-parametric estimate of  $d(G(x); G, F)$ , i.e.,

$$\hat{\hat{d}}(G(x); G, F) = (1 - \hat{\eta}) \frac{\hat{f}_b(x)}{f_s(x, \hat{\theta}_s)} + \hat{\eta}, \quad (34)$$

and rewrite

$$\begin{aligned}\widehat{f}_b(x) &= \frac{\widehat{f}_b(x)\widehat{d}(G(x);G,F) - \widehat{\eta}f_s(x,\widehat{\theta}_s)}{(1 - \widehat{\eta})} \\ \widehat{f}_s(x) &= \frac{\widehat{f}_b(x)\widehat{d}(G(x);G,F) - (1 - \widehat{\eta})\widehat{f}_b(x)}{\widehat{\eta}}.\end{aligned}\quad (35)$$

In the upper right panel of Fig. 5, the true comparison density (grey dashed line) for our physics sample is compared with its semiparametric estimate computed as in (34) (pink dashed line) with  $f_s(x, \widehat{\theta}_s) = f_s(x)$  in (13). The graphs of two nonparametric estimates of  $d(u; G, F)$  computed via (8) with  $M = 4$  and  $M = 9$  (blue chained line and black dotted line), respectively, are added to the same plot. Not surprisingly, incorporating the information available on the signal distribution drastically improves the accuracy of the analysis. The semiparametric estimate matches  $d(u; G, F)$  almost exactly, whereas both nonparametric estimates show some discrepancies from the true comparison density. All the estimates suggest that there is only one prominent peak in correspondence of the signal region.

When moving from the comparison density domain to the density domain in Fig. 4, the discrepancies between the nonparametric estimates and the true density  $f(x)$  are substantially magnified. Specifically, when computing (8) and (10) with  $M = 4$  (blue chained line), the height signal peak is underestimated whereas, when choosing  $M = 9$ , the  $\widehat{f}(x)$  exhibits high bias at the boundaries<sup>5</sup> (dotted black line).

**Case IIb: background + (unknown) signal.** When the signal distribution is unknown, the CD plot of  $\widehat{d}(u; G, F)$  can be used to guide the scientist in navigating across the different theories on the astrophysical phenomenon under study and specify a suitable model for the signal, i.e.,  $f_s$ . The model proposed can then be validated, as in Case IIa, by fitting (33) and constructing deviance tests and CD plots.

At this stage, the scientist has the possibility to iteratively query the data and explore the distribution of the signal by assuming different models. A viable signal characterization is achieved when no significant deviations of  $\widehat{d}(u; G_{bs}, F)$  from one are observed (e.g., see upper left panel of Fig. 5). Notice that a similar approach can be followed also in the background calibration stage (Section V A) to provide a parametric characterization of the background distribution.

**Case III: background + (known) signal + unexpected source.** The tools proposed so far can also be used to detect signals from unexpected sources whose pdfs are, by design, unknown.

Suppose that the physics sample  $x$  contains  $n = 1300$  observations whose true (unknown) pdf  $f(x)$  is equal to  $f_{bsh}(x)$

$$f_{bsh}(x) = (1 - \eta_1 - \eta_2)f_b(x) + \eta_1f_s(x) + \eta_2f_h(x) \quad (36)$$

<sup>5</sup> Boundary bias is a common problem among nonparametric density estimation procedures [e.g., 17, Ch.5, Ch.8]. When aiming for a non-parametric estimate of the data density  $f(x)$ , solutions exist to mitigate this problem [e.g., 24].

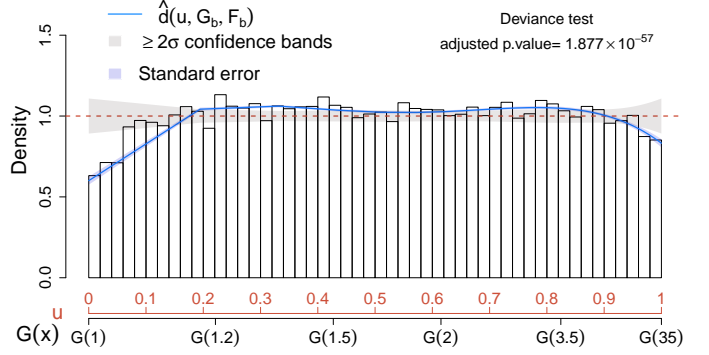


FIG. 6: Deviance test and CD plot for the source-free simulated Fermi-LAT sample.

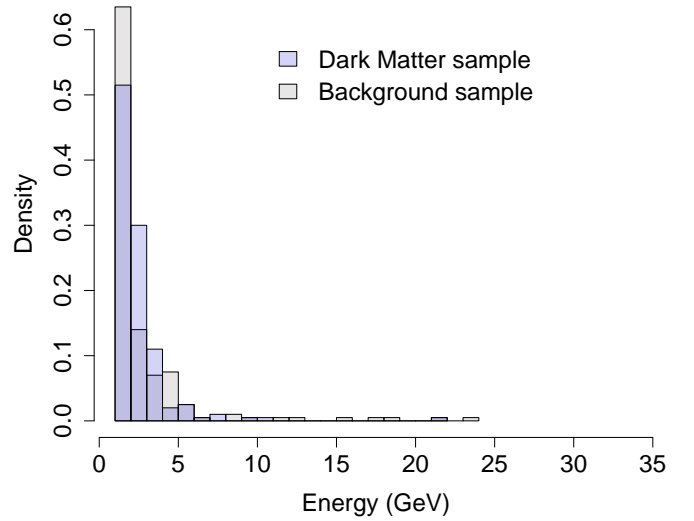


FIG. 7: Histogram of two simulated Fermi-LAT physics samples of  $n = 200$  observations. The grey histogram corresponds to the background-only sample, whereas the blue histogram corresponds to the dark matter signal sample.

where  $f_h(x)$  is the pdf of the unexpected signal and assume its distribution to be normal with center at 37 and width 1.8. Let  $f_b(x)$  and  $f_s(x)$  be defined as in (11) and (13), respectively, and let  $\eta_1 = 0.15$  and  $\eta_2 = 0.1$ .

We can start with a nonparametric signal detection stage by setting  $g(x) = \widehat{g}_{bs}(x)$  in (30), with  $f_s$  defined as in (13) and  $\widehat{\eta}$  estimated via MLE. The respective CD plot and deviance tests are reported in the bottom left panel of Fig. 5. Choosing  $M = 9$ , as in (27), both the CD plot and deviance test indicate a significant departure from the expected background-only model and a prominent peak is observed in correspondence of the signal of interest centered around 25. A second but weaker peak appears to be right on the edge of our confidence bands, suggesting the possibility of an additional source. At this stage, if  $f_s$  was unknown, we could proceed with a semiparametric signal characterization as in Case IIb.

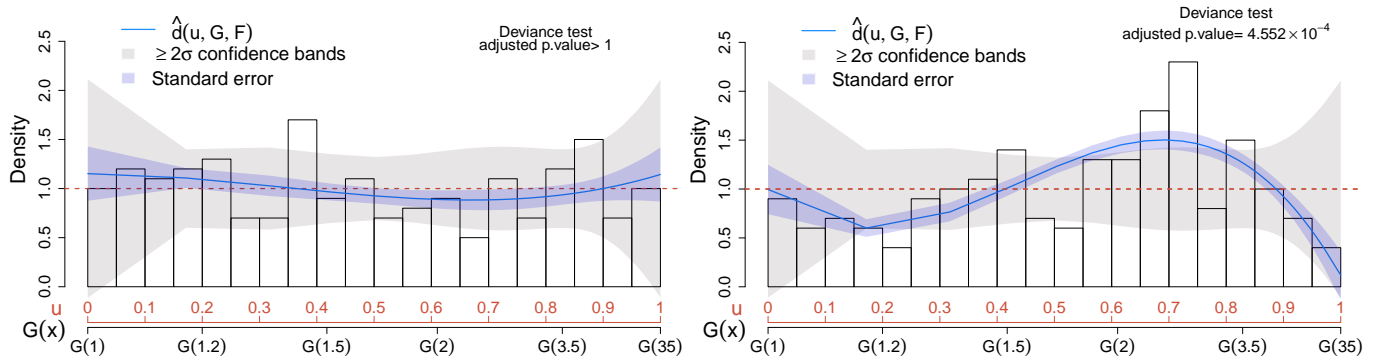


FIG. 8: Deviance test and CD plots for the simulated Fermi-LAT background-only sample of size 200 (left panel) and the simulated Fermi-LAT dark matter signal sample of size 200 (right panel). In both cases, the postulated distribution  $G$  corresponds to the cdf of the calibrated background model in (38). For the sake of comparison,  $d(u; G, F)$  has been estimated via (8), with  $M = 3$  in both cases.

Whereas assuming that the distribution of the signal of interest is known and given by (13), we fit (33), aiming to capture a significant deviation in correspondence of the second bump. This is precisely what we observe in the bottom right panel of Fig. 5. Here the estimated comparison density deviates from (30) around 35, providing evidence in favor of an additional signal in this region. We can then proceed as in Case IIb by exploring the theories available and/or collecting more data to further investigate the nature and the cause of the unanticipated bump.

## VI. BACKGROUND MISMODELLING DUE TO INSTRUMENTAL NOISE AND SIGNAL DETECTION ON SMALL SAMPLES

When conducting real data analyses one has to account that the data generating process is affected by both statistical and non-random uncertainty due to the instrumental noise. As a result, even when a model for the background is known, the data distribution may deviate from it due to the smearing introduced by the detector [e.g., 26]. In order to account for the instrumental error affecting the data, it is common practice to consider folded distributions where the errors due to the detector are often modelled assuming a normal distribution or estimated via non-parametric methods [e.g., 27, 28]. Here, it is shown how the same approach described in Sections V A and V B 1 can be used to account for background mismodelling due to ignoring the instrumental noise.

The data considered come from a simulated observation by the Fermi Large Area Telescope [29] with realistic representations of the effects of the detector and present backgrounds [30, 31]. The Fermi-LAT is a pair-conversion  $\gamma$ -ray telescope on board the earth-orbiting Fermi satellite. It measures energies and images  $\gamma$ -rays between about a 100 MeV and several TeV. The goal of the analysis is to assess if the data could result from the self-annihilation of a dark matter particle.

First, we calibrate our “folded” background distribution over a source-free sample of 35,157 i.i.d. observations from a

power-law distributed background source with index 2.4 (i.e.,  $\phi = 1.4$  in (37)) and contaminated by instrumental errors of unknown distribution. Let the distribution of the astrophysical background be

$$g_b(x) = \frac{1}{k_\phi x^{\phi+1}} \quad (37)$$

where  $k_\phi$  is a normalizing constant and  $x \in [1, 35]$  Giga electron Volt (GeV). We proceed by fitting (37) via maximum likelihood and setting it as postulated background distribution; this is equivalent to assuming that the effect of the detector is irrelevant. We then estimate  $d(G_b(x); G_b, F_b)$  and  $f_b$  as in (8) and (14) respectively, with  $M = 4$  (and chosen as in Section IV C). The deviance tests and CD plot are reported in Fig. 6. The resulting estimate for the background distribution is

$$\begin{aligned} \hat{f}_b(x) = & \frac{1}{k_{\hat{\phi}} x^{\hat{\phi}+1}} \left( 1 + 0.027 \text{Leg}_1[G_b(x)] - 0.067 \text{Leg}_2[G_b(x)] \right. \\ & \left. + 0.026 \text{Leg}_3[G_b(x)] - 0.045 \text{Leg}_4[G_b(x)] \right), \end{aligned} \quad (38)$$

where  $G_b(x)$  is the cdf of (37) and  $\hat{\phi} = 1.3589$  is the ML estimate of  $\phi$  in (37).

Second, we proceed with the signal detection phase by setting  $g(x) = \hat{f}_b(x)$ . Similarly to Section V B 1, two physics samples are given; one containing 200 observations from the background source distributed, as in (37), and the other containing 200 observations from a dark matter emission. The signal distribution from which the data have been simulated is the pdf of  $\gamma$ -ray dark matter energies in [32, Eq. 28]. Both physics samples include the contamination due to the instrumental noise, and the respective histograms are shown in Fig. 7.

The selection scheme in Section IV C suggests that no significant departure from (38) occurs on the background-only physics sample, whereas, for the signal sample, the strongest significance is observed at  $M = 3$ ; therefore, for the sake of

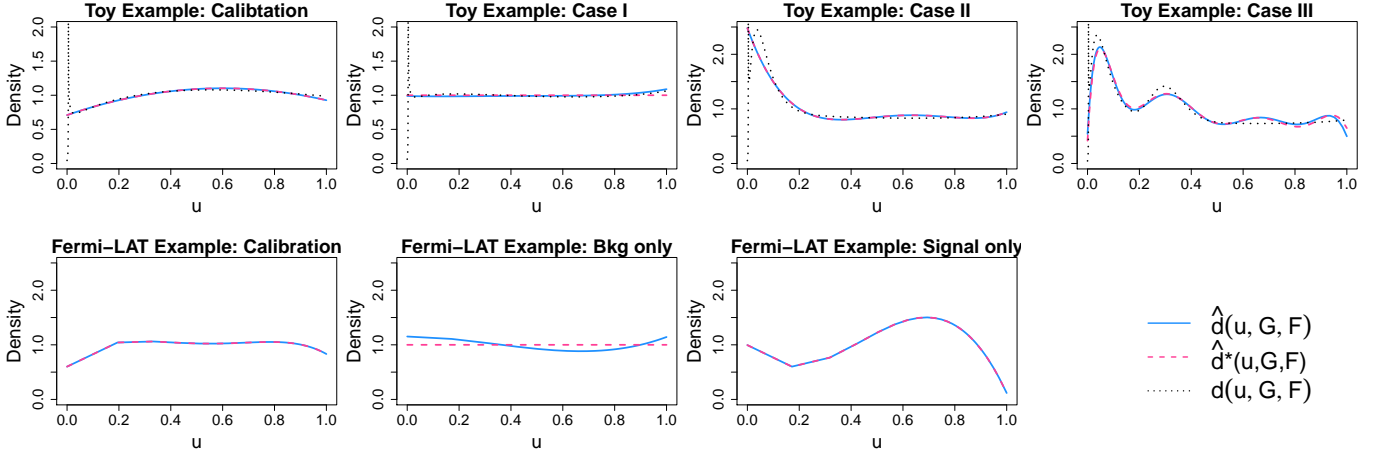


FIG. 9: Comparison of the estimators  $\hat{d}(u; G, F)$  (blue solid lines) and  $\hat{d}^*(u; G, F)$  (pink dashed lines) for the toy example in Section III and the Fermi-LAT analysis in Section VI. When available, the true comparison densities  $d(u; G, F)$  are displayed as dotted black curves.

comparison, we choose  $M = 3$  in both cases. The respective deviance tests and CD plots are reported in Fig. 8. As expected, the left panel of Fig. 8 shows a flat estimate of the comparison density on the background-only sample. Conversely, the right panel of Fig. 8 suggests that an extra bump is present over the  $[2, 3.5]$  region with  $3.318\sigma$  significance (adjusted p-value= $4.552 \cdot 10^{-4}$ ). As in (34), it is possible to proceed with the signal characterization stage; however, in this setting, one has to account for the fact that also the signal distribution must include the smearing effect of the detector.

## VII. MODEL-DENOISING

When dealing with complex background distributions, a large value of  $M$  may be necessary to reduce the bias of the estimated comparison density. However, since larger values of  $M$  lead to rough approximation of the true density, it is often convenient to denoise the estimator in (8). Section VII A reviews the model-denoising approach proposed by [8, 9], whereas Section VII B briefly discusses inference and model selection in this setting. Finally, Section VII C compares the results obtained with a full and a denoised solution on the examples in Sections V and VI.

### A. AIC denoising

Let  $\widehat{LP}_1, \dots, \widehat{LP}_M$  be the estimate of the first  $M$  coefficients of the expansion in (4). The most “significant”  $LP_j$  coefficients are selected by sorting the respective  $\widehat{LP}_j$  estimates so that

$$\widehat{LP}_{(1)}^2 \geq \widehat{LP}_{(2)}^2 \geq \dots \geq \widehat{LP}_{(M)}^2$$

and choosing the value  $k = 1, \dots, M$  for which  $AIC(k)$  in (39) is maximum

$$AIC(k) = \sum_{j=1}^k \widehat{LP}_{(j)}^2 - \frac{2k}{n}. \quad (39)$$

The AIC-denoised estimator of  $d(u; G, F)$  is given by

$$\hat{d}^*(u; G, F) = 1 + \sum_{j=1}^{k_M^*} \widehat{LP}_{(j)} \text{Leg}_{(j)}(u) \quad (40)$$

where  $\widehat{LP}_{(j)}$  is the estimate whose square is the  $j^{\text{th}}$  largest among  $\widehat{LP}_1^2, \dots, \widehat{LP}_M^2$ ,  $\text{Leg}_{(j)}(u)$  is the respective shifted Legendre polynomial and

$$k_M^* = \underset{k}{\text{argmax}} \{AIC(1), \dots, AIC(M)\}. \quad (41)$$

*Practical remarks.* Recall that the first  $M$  coefficients  $LP_j$  can be expressed as a linear combination of the first  $M$  moments of  $U$ . Thus, the AIC-denoising approach selects the  $LP_j$  coefficients which carry all the “sufficient” information on the first  $M$  moments of the distribution.

### B. Inference after denoising

The deviance test can be used, as in Section IV C, to choose the size of the initial basis of  $M$  polynomials among  $M_{\text{max}}$  possible models. Finally, the  $k_M^*$  largest coefficients are chosen by maximizing (39). This two-step procedure selects  $\hat{d}^*(u; G, F)$  in (40) from a pool of  $M_{\text{tot}} = M_{\text{max}} + \frac{M(M-1)}{2}$  possible estimators. Therefore, the Bonferroni-adjusted p-value of the deviance test is given by

$$M_{\text{tot}} \cdot P(\chi_{k_M^*}^2 > d_{k_M^*}) \quad (42)$$

	$M, k_M^*$ selected	Method	Deviance p-values	Adjusted p-values
<b>Toy example Calibration</b>	$M = 2$ $k_2^* = 2$	Full	$p(2) = 3.199 \cdot 10^{-12}$	$20 \cdot p(2) = 6.397 \cdot 10^{-11}$
		Denoisied	$p(2) = 3.199 \cdot 10^{-12}$	$21 \cdot p(2) = 6.717 \cdot 10^{-11}$
<b>Toy example Case I</b>	$M=18$ $k_{18}^* = 2$	Full	$p(18) = 0.2657$	$20 \cdot p(18) > 1$
		Denoisied	$p(2) = 5.096 \cdot 10^{-4}$	$21 \cdot p(2) = 0.0882$
<b>Toy example Case II</b>	$M = 4$ $k_4^* = 4$	Full	$p(4) = 8.994 \cdot 10^{-33}$	$20 \cdot p(4) = 1.799 \cdot 10^{-31}$
		Denoisied	$p(4) = 8.994 \cdot 10^{-33}$	$21 \cdot p(4) = 2.338 \cdot 10^{-31}$
<b>Toy example Case III</b>	$M = 9$ $k_9^* = 6$	Full	$p(9) = 2.590 \cdot 10^{-28}$	$20 \cdot p(9) = 5.181 \cdot 10^{-27}$
		Denoisied	$p(6) = 4.457 \cdot 10^{-30}$	$35 \cdot p(1) = 2.496 \cdot 10^{-28}$
<b>Fermi-LAT example Calibration</b>	$M = 4$ $k_4^* = 4$	Full	$p(4) = 9.383 \cdot 10^{-59}$	$20 \cdot p(4) = 1.877 \cdot 10^{-57}$
		Denoisied	$p(4) = 9.383 \cdot 10^{-59}$	$26 \cdot p(4) = 2.440 \cdot 10^{-57}$
<b>Fermi-LAT example Bkg only sample</b>	$M = 16$ $k_{16}^* = 4$	Full	$p(16) = 0.2080$	$20 \cdot p(16) > 1$
		Denoisied	$p(4) = 0.0043$	$26 \cdot p(4) = 0.6076$
<b>Fermi-LAT example Calibration</b>	$M = 3$ $k_3^* = 3$	Full	$p(3) = 2.276 \cdot 10^{-5}$	$20 \cdot p(3) = 4.552 \cdot 10^{-4}$
		Denoisied	$p(3) = 2.276 \cdot 10^{-5}$	$21 \cdot p(3) = 5.235 \cdot 10^{-4}$

TABLE I: Model selection and inference for the toy example in Section III and the Fermi-LAT analysis in Section VI. The second column reports the  $M$  and  $k_M^*$  values selected as in (27) and (41), respectively. The third column collects the unadjusted deviance p-values for the full and denoisied solutions. The Bonferroni-adjusted p-values, computed as in (28) and (42) are reported in the fourth column. The correction terms applied correspond to  $M_{\max} = 20$  for the full solution and

$$M_{\text{tot}} = M_{\max} + \frac{M(M-1)}{2} \text{ for the denoisied solution.}$$

with  $d_{k_M^*} = \sum_{j=1}^{k_M^*} \widehat{LP}_{(j)}^2$ . Similarly, confidence bands can be constructed as

$$\left[ 1 - c_{\alpha, M_{\text{tot}}} \sqrt{\sum_{j=1}^{k_M^*} \frac{1}{n} \text{Leg}_{(j)}^2(u)}, 1 + c_{\alpha} \sqrt{\sum_{j=1}^{k_M^*} \frac{1}{n} \text{Leg}_{(j)}^2(u)} \right] \quad (43)$$

where  $c_{\alpha, M_{\text{tot}}}$  is the solutions of

$$2(1 - \Phi(c_{\alpha, M_{\text{tot}}})) + \frac{k_0}{\pi} e^{-0.5c_{\alpha, M_{\text{tot}}}^2} = \frac{\alpha}{M_{\text{tot}}}. \quad (44)$$

### C. Comparing full and denoisied solution

Fig. 9 compares the fit of the estimators  $\widehat{d}(u; G, F)$  and  $\widehat{d}^*(u; G, F)$  for the examples in Sections V and VI. For all the cases considered,  $M$  and  $k_M^*$  have been selected as in (27) and (41) (see second column of Table I). When no significance was achieved for any of the values of  $M$  considered, a small basis of  $M = 3$  or  $M = 4$  polynomials was chosen for the full estimator  $\widehat{d}(u; G, F)$ , which was then further denoisied in order to obtain  $\widehat{d}^*(u; G, F)$ . Table I shows the results of the deviance tests of the full and the denoisied solution for the examples in Sections V and VI. The unadjusted p-values and the Bonferroni-adjusted p-values are reported in the second and third columns, respectively. In most cases,  $k_M^* = M$  and the estimators  $\widehat{d}(u; G, F)$  and  $\widehat{d}^*(u; G, F)$  overlap over the entire

range  $[0, 1]$ . The inferential results were also approximately equivalent in the majority of the situations considered.

The main differences are observed in the analysis of the background-only physics samples for both the toy example (Case I) and the Fermi-LAT example. In both cases, the deviance-selection procedure leads to non-significant results for all the values of  $M$  considered. The minimum p-values are observed for  $M = 18$  (unadjusted p-value=0.2657) for the toy example and at  $M = 16$  (unadjusted p-value=0.2080) for the Fermi-LAT example. However, in this setting, the denoising process leads to  $k_{18}^* = 2$  and  $k_{16}^* = 4$ , and the respective unadjusted p-values are given by  $5.096 \cdot 10^{-4}$  and  $0.0043$ . This further emphasizes the importance of adjusting for model selection in order to avoid false discoveries. For modelling purposes and for the sake of comparison with the case where a signal is present, a basis of  $M = 4$  and of  $M = 3$  was chosen for the toy and the Fermi-LAT examples, respectively. Since in both cases the true distribution of the data is the same as the postulated one, the denoising process sets all the coefficients equal to zero ( $k_M^* = 0$ ).

For Case III of the toy example, only  $k_M^* = 6$  out of  $M = 9$  coefficients are selected when denoising (see Table I). Despite the upper right panel of Fig. 9 showing that the full and the denoisied solution are almost overlapping, the latter leads to an increased sensitivity (adjusted p-value= $2.496 \cdot 10^{-28}$ ) compared to the full solution (adjusted p-value= $5.181 \cdot 10^{-27}$ ).

These results suggest that the denoising approach can easily adapt to situations where a sparse solution is preferable



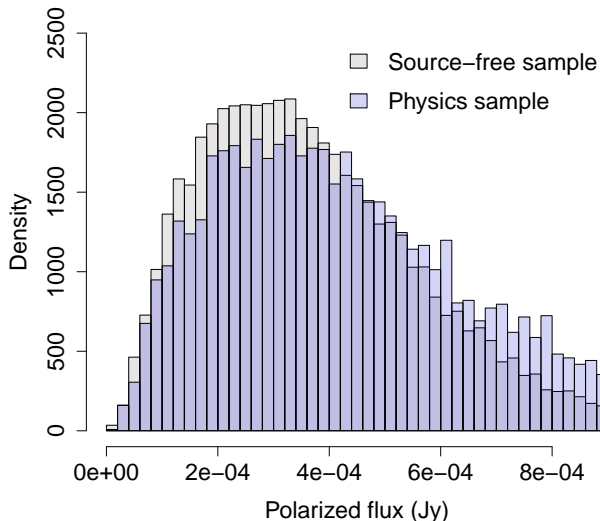


FIG. 10: Histograms of the NVSS samples. The source-free sample (grey histogram) contains  $N = 28,739$  observations obtained over four different control regions. The physics sample (blue histogram) contains  $n = 6220$  observations from the source location.

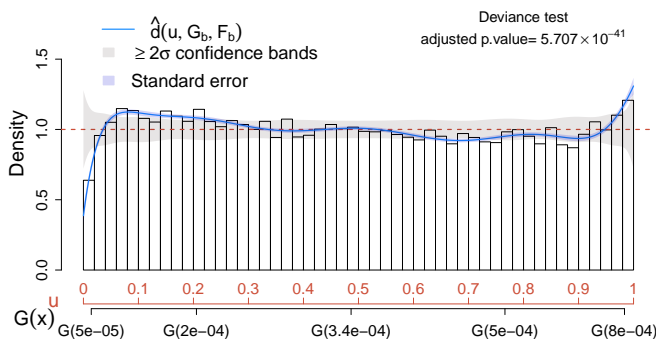


FIG. 11: Deviance test and CD plot for the NVSS source-free sample of size 28,739 compared to the Rayleigh distribution in (45).

(i.e., when only few of the  $M$  coefficients  $LP_j$  are non-zero) without enforcing sparsity when many of the  $M$  coefficients considered are needed to adequately fit the data (e.g., bottom right panel of Fig. 9). From an inferential perspective, denoising can improve the sensitivity of the analysis; however, in order to avoid false discoveries, extra care needs to be taken when the deviance selection procedure leads to large p-values for all the  $M_{\max}$  models considered.

## VIII. AN APPLICATION ON STACKING EXPERIMENTS

In radio astronomical surveys, stacking techniques are often used to combine noisy images or “stacks” in order to increase the signal-to-noise ratio and improve the sensitivity of

the analysis in detecting faint sources [e.g., 33–35]. In polarized signal searches, for instance, a faint population of sources is considered when the median polarized intensity observed over control regions differs significantly from the median of the region where the sources are expected to be present. In this context, the distribution of the intensity of the source polarization is often assumed to be Rician, and it reduces to a Rayleigh distribution when no signal is present [36]. Below, it is shown how the methods described in Sections V A and V B 1 can be used to assess whether the Rayleigh distribution is a reliable model for the background and investigate the impact of incorrectly assuming a Rayleigh distribution on the sensitivity of the analysis.

The data considered comes from the NRAO VLA Sky Survey (NVSS) [37]. The NVSS is an astronomical survey of the Northern hemisphere carried out by the Very Large Array of the National Radio Astronomy Observatory. The NVSS has detected 1.8 million sources in total intensity, but only 14% of these have a reported a peak polarized signal greater than  $3\sigma$  [35]. A physics sample of 6,220 observations has been selected from positions where compact radio sources with a brightness in total intensity between 15 and 25 milliJansky are known to be present, whereas a source-free sample of size 28,739 was collected from four different control regions for each source. Both samples are assumed to be i.i.d. In order to mitigate the effect of the outliers,<sup>6</sup> the analysis has been limited to the region  $[0, 0.0009]$  Jansky (Jy) in polarized flux. The histograms of the source-free and signal samples considered are shown in Fig. 10.

As first step, we fit a Rayleigh distribution (adequately truncated over the range  $[0, 0.0009]$ ) on the source-free sample, i.e.,

$$g_b(x) = \frac{x e^{-\frac{x^2}{2\hat{\sigma}^2}}}{k_{\hat{\sigma}^2}} \quad (45)$$

where  $k_{\hat{\sigma}^2}$  is a normalizing constant,  $\hat{\sigma} = 0.0003$  is the ML estimate of the unknown parameter  $\sigma$ , and  $x \in [0, 0.0009]$  Jy. In order to assess if (45) provides a good fit for the data, we estimate the comparison density  $d(G_b(x); G_b, F_b)$  by, first, selecting  $M$  as in (27) and then applying the AIC-based denoising approach described in Section VII A. In this case, the denoised solution selects  $k^* = 9$  out of  $M = 10$  polynomial terms. The deviance tests and the CD plot in Fig. 11 suggest that, despite the fact that the median of the data coincides with the one of the Rayleigh model, overall, the latter does not provide a good fit for the distribution of the source-free sample. Specifically, the data distribution shows a higher right tail than one expected under the Rayleigh assumption, whereas the first quantiles are overestimated by the Rayleigh. Therefore, the researcher can either decide to use a more refined parametric model for the background or consider the calibrated background distribution of the form in (14), which in our setting

<sup>6</sup> In statistics, an observation  $x_i$  is considered an outlier if  $x_i < Q_{0.25} - 1.5[Q_{0.75} - Q_{0.25}]$  or  $x_i > Q_{0.75} + 1.5[Q_{0.75} - Q_{0.25}]$  where  $Q_{0.25}$  and  $Q_{0.75}$  are the first and the third sample quartiles.

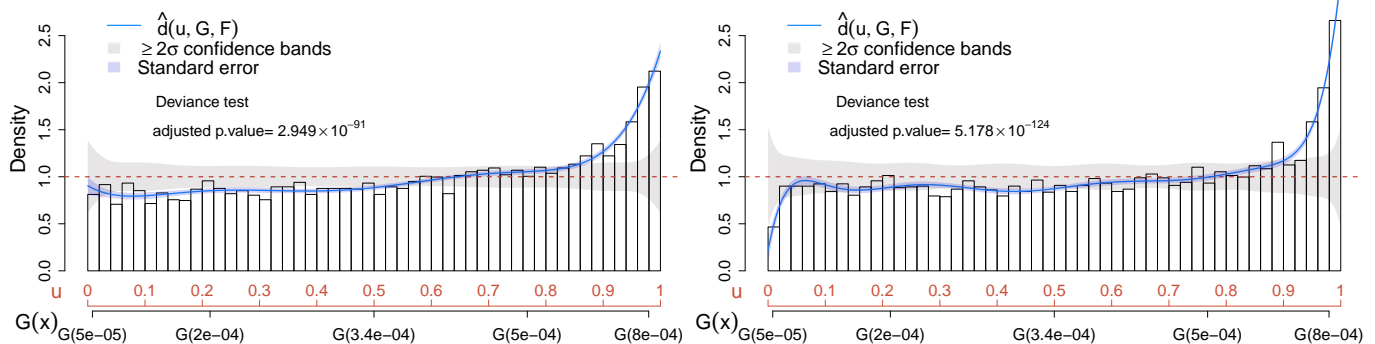


FIG. 12: Deviance tests and CD plots for the NVSS physics sample assuming  $g(x)$  to be the calibrated background model in (46) (left panel) and when letting  $g(x)$  be the pdf in of the truncated Rayleigh distribution in (45). In both cases the estimator of the comparison density has been denoised as described in Section VII A. The values of  $M$  and  $k^*$  considered are  $M = k^* = 6$  and  $M = 9, k^* = 8$  for the estimators on the left and right panels, respectively.

specifies as

$$\begin{aligned} \hat{f}_b(x) = & \frac{xe^{-\frac{x^2}{2\sigma^2}}}{k_{\hat{\sigma}^2}} \left( 1 - 0.018\text{Leg}_1[G_b(x)] + 0.012\text{Leg}_2[G_b(x)] \right. \\ & + 0.052\text{Leg}_3[G_b(x)] - 0.014\text{Leg}_4[G_b(x)] + 0.047\text{Leg}_5[G_b(x)] \\ & - 0.018\text{Leg}_6[G_b(x)] + 0.031\text{Leg}_7[G_b(x)] + 0.016\text{Leg}_9[G_b(x)] \\ & \left. - 0.015\text{Leg}_{10}[G_b(x)] \right), \end{aligned} \quad (46)$$

where  $G_b(x)$  is the cdf of (45).

The strategy described in Section VB 1 allows us to identify where significant differences between the control and source sample occur. In order to assess the effect of incorrectly assuming a Rayleigh background, we compare the distribution of the physics sample with both the Rayleigh and the calibrated background distribution in (46). Figure 12 reports deviance tests and CD plots obtained on the physics sample when setting  $g(x) = \hat{f}_b(x)$  in (45) (left panel) and  $g(x) = \hat{f}_b(x)$  in (46) (right panel). Both analyses provide strong evidence that the distribution of the physics sample differs significantly from the postulated models  $\hat{f}_b(x)$  and  $g_b(x)$ , and the most substantial discrepancies occur on the right tail of the distribution. However, since the Rayleigh model underestimates the right tail of the background distribution (see Fig. 11), it leads to an artificially enhanced sensitivity in this region. The differences between the two CD plots are less prominent around the median expected under  $\hat{f}_b(x)$  and  $g_b(x)$  (i.e., in correspondence of  $u = 0.5$  in both plots).

This suggests that, for these data, assuming a background Rayleigh distribution would not substantially affect the results of a comparison based on the median; however, focusing solely on the median can strongly affect the overall sensitivity of the analysis since the major differences occur at the higher quantiles of the distribution. Conversely, the calibrated background model in (46) allows us to safely compare the entire distribution of the polarized intensity in the source and control regions via CD plots and deviance tests without compromis-

ing the sensitivity of the analysis.

## IX. DISCUSSION

This article proposes a unified framework for signal detection and characterization under background mismodelling. From a methodological perspective, the methods presented here extend the classical LP modelling framework to the inferential setting.

The solution discussed is articulated in two main phases: a calibration phase where the background model is “trained” on a source-free sample and a signal search phase conducted on the physics sample collected by the experiment. If a model for the signal is given, the method proposed allows the identification of hidden signals from new unexpected sources and/or the refining of the postulated background or signal distributions. Furthermore, the tools presented in this manuscript can be easily extended to situations where a source-free sample is not available and the background is unknown (up to some free parameters); however, in this setting the signal distribution is required to be known, and the physics sample is expected to contain background observations or signal observations only.

The analyses in Section V have highlighted that, despite a fully non-parametric approach provides reliable inference, it may lead to unsatisfactory estimates when the postulated pdf  $g$  is substantially different from the true density  $f$ . In this setting, a semiparametric stage can be performed in order provide a reliable model for the data.

Each individual step in both the nonparametric and the semiparametric stage provides useful scientific insights on the nature of the signal(s) and the background. Hence, an automatized implementation of the steps of Algorithm 1 (including decisions based only on the p-values of the deviance tests) is discouraged as it would lead to a substantial loss of scientific knowledge on the phenomena under study.

Finally, it is important to point out that, despite this article’s focus on the one-dimensional searches on continuous data, all the constructs presented in Sections II and IV also apply to

the discrete case when considering i.i.d. events. More work is needed to extend these results to searches in multiple dimensions and when considering Poisson events with functional mean.

### CODE AVAILABILITY

The R code and functions needed to implement the tools described in this manuscript are available at <http://salgeri.umn.edu/my-research>. A detailed tutorial on how to use the functions provided in R is also available at the same link.

### ACKNOWLEDGMENTS

The author thanks Jeroen Stil, who provided the NVSS datasets used in Section VIII, and Lawrence Rudnick, who first recognized the usefulness of the method proposed in the context of stacking experiments. Conversations with Subhadeep Mukhopadhyay have been of great help when this work was first conceptualized. Discussions and e-mail exchanges with Charles Doss and Chad Shafer are gratefully acknowledged.

- 
- [1] Aprile, E., et al. *Physical review letters* 119.18 (2017): 181301.
  - [2] Agnese, R., et al. *arXiv preprint arXiv:1808.09098* (2018).
  - [3] Smith, R., and Eric T. *Physical Review X* 8.2 (2018): 021019.
  - [4] CMS Collaboration. *arXiv preprint arXiv:1811.08459* (2018).
  - [5] Yellin, S. *Physical Review D* 66.3 (2002): 032005.
  - [6] Priel, N., et al. *Journal of Cosmology and Astroparticle Physics* 2017.05 (2017): 013.
  - [7] Dauncey, P. D., et al. *Journal of Instrumentation* 10.04 (2015): P04015.
  - [8] Mukhopadhyay, S., and Parzen, E. *arXiv preprint arXiv:1405.2601* (2014).
  - [9] Mukhopadhyay, S. *Electronic Journal of Statistics* 11.1 (2017): 215-240.
  - [10] Mukhopadhyay, S., and Douglas F. *Scientific reports* 8.1 (2018): 9983.
  - [11] Mukhopadhyay, S., and Parzen, E. *Journal of Risk and Financial Management* 11.3 (2018): 37.
  - [12] Mukhopadhyay, S. *Biometrics* 72.2 (2016): 325-334.
  - [13] Mukhopadhyay, S. *Journal of Nonparametric Statistics* 30.4 (2018): 1003-1015.
  - [14] Parzen, E. *Asymptotic methods in probability and statistics*. North-Holland, 1998. 611-617.
  - [15] Anderson, T.W., and Darling, D.A. *The annals of mathematical statistics* 23.2 (1952): 193-212.
  - [16] Shapiro, S.S. and Wilk, M.B. *Biometrika* 52.3/4 (1965): 591-611.
  - [17] Wasserman, L. *All of nonparametric statistics*. Springer Science & Business Media (2006).
  - [18] Provost, S.B. *Mathematica Journal* 9.4 (2005): 727-756.
  - [19] Provost, S., and Jiang, M. *International Journal of Computational and Mathematical Sciences* 6 (2012): 12-29.
  - [20] Pilla, R.S., Loader, C. and Taylor, C.C. *Physical review letters* 95.23 (2005): 230202.
  - [21] Shen, X., Huang, H.C., and Ye, J. *Journal of the American Statistical Association* 99.467 (2004): 751-762.
  - [22] Leeb, H., and Ptscher, B.M. *Econometric Theory* 21.1 (2005): 21-59.
  - [23] Bonferroni, C.E. *Teoria statistica delle classi e calcolo delle probabilita*. Libreria internazionale Seeber, 1936.
  - [24] Efromovich, S. *Nonparametric Curve Estimation*. Springer Science & Business Media, 2008.
  - [25] Lyons, Louis. *PHYSTAT 2011 Workshop proceedings* (2011): 225-228.
  - [26] Lyons, L. *PHYSTAT 2011 Workshop proceedings* (2011): 225-228.
  - [27] Panaretos, V. *PHYSTAT 2011 Workshop proceedings* (2011): 229-239.
  - [28] Blobel, Volker. *PHYSTAT 2011 Workshop proceedings* (2011): 240-251.
  - [29] Atwood W. B. et al. *The Astrophysical Journal* (2009): 697 2.
  - [30] Algeri, S., et al. *Journal of Instrumentation* 11.12 (2016): P12010.
  - [31] Algeri, S., Conrad, J. and van Dyk, D.A. *Monthly Notices of the Royal Astronomical Society: Letters* 458.1 (2016): L84-L88.
  - [32] Bergstrm, L., Ullio, P. and Buckley, J.H. *Astroparticle Physics* 9.2 (1998): 137-162.
  - [33] Brown, S., et al. *The Astrophysical Journal Letters* 740.1 (2011): L28.
  - [34] White, R.L., et al. *The Astrophysical Journal* 654.1 (2007): 99.
  - [35] Stil, J. M., et al. *The Astrophysical Journal* 787.2 (2014): 99.
  - [36] Simmons, J. F. L., and B. G. Stewart. *Astronomy and Astrophysics* 142 (1985): 100-106.
  - [37] Condon, J.J., et al. *The Astronomical Journal* 115.5 (1998): 1693.